JCTC Journal of Chemical Theory and Computation

ARTICLE

pubs.acs.org/JCTC

Microscopic Symmetry Imposed by Rotational Symmetry Boundary Conditions in Molecular Dynamics Simulation

Amitava Roy and Carol Beth Post*

Medicinal Chemistry and Molecular Pharmacology, Purdue University, West Lafayette, Indiana, United States

Supporting Information

ABSTRACT: A large number of viral capsids, as well as other macromolecular assemblies, have an icosahedral structure or structures with other rotational symmetries. This symmetry can be exploited during molecular dynamics (MD) to model in effect the full viral capsid using only a subset of primary atoms plus copies of image atoms generated from rotational symmetry boundary conditions (RSBC). A pure rotational symmetry operation results in both primary and image atoms at short-range, and within nonbonded interaction distance of each other, so that nonbonded interactions cannot be specified by the minimum image convention and explicit treatment of image atoms is required. As such, an unavoidable consequence of RSBC is that the enumeration of nonbonded interactions in regions surrounding certain rotational axes must include both a primary atom and its copied image atom, thereby imposing microscopic symmetry for some forces. We examined the possibility of artifacts arising from this imposed microscopic symmetry of RSBC using two simulation systems: a water shell and human rhinovirus 14 (HRV14) capsid with explicit water. The primary unit was a pentamer of the icosahedron, which has the advantage of direct comparison of icosahedrally equivalent spatial regions, for example regions near a 2-fold symmetry axis with imposed symmetry and a 2-fold axis without imposed symmetry. An analysis of structural and dynamic properties of water molecules and protein atoms found similar behavior near symmetry axes with imposed symmetry and where the minimum image convention fails compared with that in other regions in the simulation system, even though an excluded volume effect was detected for water molecules near the axes with imposed symmetry. These results validate the use of RSBC for icosahedral viral capsids or other rotationally symmetric systems.

1. INTRODUCTION

Thousands of viruses, including those that cause human disease, have protein shells that display icosahedral symmetry. This protein shell, or viral capsid, exhibits remarkable physical properties,[1,2] which are necessary to promote the virus life cycle. These properties and their functional role in viral pathogenesis have long captured the interest of experimental and computational researchers.

All-atom MD simulations provide the most rigorous and detailed computational approach to investigate capsid physical behavior. An entire capsid solvated in water consists of ~2 million or more atoms. Simulation of such a large system is generally impractical even though a few notable exceptions have been reported.[3,4] The capsid of human rhinovirus, one of the smallest RNA viruses, has ~500 000 atoms, and its diameter is ~300 Å. The computational time for MD simulation can be reduced by exploiting the rotational symmetry of viruses.[5−8] Other macromolecular assemblies, such as the icosahedral pyruvate dehydrogenase complex,[9] also display rotational symmetry, as symmetry often confers stability and results in economical usage of basic components.[10] Simulation of these systems can also exploit rotational symmetry to reduce computation time. In the case of icosahedral viruses with three protomers in each of the 20 triangular tiles of an icosahedron, periodic boundary conditions allow simulation of as little as 1/60th of the entire capsid while retaining effects of the whole virus particle.[5−8]

With periodic boundary conditions, a primary set of atoms is replicated to produce a neighboring set of atoms and so model the effect of a larger system. Symmetry related coordinates are generated by the transformation of atoms composing the primary unit to image atoms in the neighboring units as follows:

$$\mathbf{x}(k') = \mathbf{R}\cdot\mathbf{x}(k) \quad (1)$$

where $\mathbf{R}$ is one of the operators of the symmetry group. The coordinates of atom k, $\mathbf{x}(k)$, are transformed to the coordinates of the image, $\mathbf{x}(k')$.

Most uses of periodic boundary conditions in simulations model infinite systems and involve open crystallographic space group symmetry with cubic, truncated octahedron, etc. primary units; however, in the case of icosahedral viruses, closed point group symmetry is used to model a finite system. Thus, we examine here the case where $\mathbf{R}$ involves pure rotational operators appropriate for viral capsids. This type of boundary condition is called rotational symmetry boundary conditions (RSBC).

Under RSBC, certain operators (eq 1) lead to short-range interactions between copies of both primary and image atoms near a rotational symmetry axis. Thus, as outlined in section 2.2, there are unavoidable occurrences of an atom in the primary unit near a rotational symmetry axis such that the distance to its own image atom (self-image) as well as distances to both primary and image atoms of neighboring atoms (replicate-image) are within the nonbonded interaction distance. The minimum image convention, typically used to evaluate nonbonded interactions in periodic boundary systems, fails in regions near such rotational symmetry axes. Nonbonded interactions must be determined by explicit treatment of image atoms as implemented with the

Received: February 5, 2011
Published: August 10, 2011

Table 1. Icosahedral Symmetry Operators[a]

	1	2	3	4	5
1	I (1,1)	F_1 (1,5)	F_2 (1,4)	F_3 (1,3)	F_4 (1,2)
2	**Z** (2,1)	ZF_1 (6,2)	ZF_2 (11,4)	ZF_3 (9,1)	ZF_4 (5,1)
3	X (3,1)	XF_1 (8,1)	XF_2 (12,1)	XF_3 (10,4)	XF_4 (7,2)
4	Y (4,1)	YF_1 (4,2)	YF_2 (4,3)	YF_3 (4,4)	YF_4 (4,5)
5	F_1Z (2,5)	F_1ZF_1 (6,1)	F_1ZF_2 (11,3)	**F_1ZF_3** (9,5)	F_1ZF_4 (5,5)
6	ZF_1Z (5,2)	ZF_1ZF_1 (2,2)	ZF_1ZF_2 (6,3)	**ZF_1ZF_3** (11,5)	ZF_1ZF_4 (9,2)
7	XF_1Z (7,1)	XF_1ZF_1 (3,5)	XF_1ZF_2 (8,5)	XF_1ZF_3 (12,5)	XF_1ZF_4 (10,3)
8	YF_1Z (3,2)	YF_1ZF_1 (8,2)	YF_1ZF_2 (12,2)	YF_1ZF_3 (10,5)	YF_1ZF_4 (7,3)
9	F_2Z (2,4)	F_2ZF_1 (6,5)	F_2ZF_2 (11,2)	F_2ZF_3 (9,4)	**F_2ZF_4** (5,4)
10	ZF_2Z (12,4)	ZF_2ZF_1 (10,2)	ZF_2ZF_2 (7,5)	ZF_2ZF_3 (3,4)	ZF_2ZF_4 (8,4)
11	XF_2Z (11,1)	XF_2ZF_1 (9,3)	XF_2ZF_2 (5,3)	XF_2ZF_3 (2,3)	**XF_2ZF_4** (6,4)
12	YF_2Z (3,3)	YF_2ZF_1 (8,3)	YF_2ZF_2 (12,3)	YF_2ZF_3 (10,1)	YF_2ZF_4 (7,4)

[a] Rotational operators of icosahedral symmetry. I is identity. $F_{1,2,3,4}$ are rotations around the 5-fold symmetry axis (OP; Figure 1) by 72°, 144°, 216°, and 288° respectively. X, Y, and Z are rotations by 180° around the X, Y, and Z axes, respectively. The first and second numbers inside the parentheses following the operator indicates the row and column numbers, respectively, of the inverse of that operator. Five operators in each row transform the protomer coordinates to five protomers for the pentameric primary unit used in this study. Neighboring images of the pentameric unit are generated by the five operators in boldface.

general image facility in the CHARMM program.[11,12] The explicit treatment of image atoms allows for the correct calculation of forces in rotationally symmetric systems; duplicate forces are avoided with the proper counting of nonbonded interactions.[11,12] While the enumeration of nonbonded interactions near such rotational symmetry axes is algorithmically correct, there is an unavoidable imposed symmetry in the forces from self-images and effects from the symmetry related to replicate images. Such microscopic symmetry is nonphysical but inherent to MD simulations under RSBC. Given the importance of RSBC for exploring molecular behavior of large systems with icosahedral symmetry, we executed an MD study to determine if artifacts on the dynamics exist with icosahedral RSBC due to the inherent microscopic symmetry on the force contributed by self-image and replicate-image interactions.

We conducted RSBC MD simulations on pure TIP3 water within a spherical shell using icosahedral symmetry and on the solvated capsid of human rhinovirus14 (HRV14). For both systems, the primary atoms in the simulation corresponded to five icosahedral asymmetric subunits or 1/12th of the icosahedron, and the symmetry-related image atoms were generated according to eq 1 from a group of five icosahedral operators. The use of this pentameric primary unit allows the operator **R** to be selected so that the minimum image convention fails at only certain rotational axes but not others (described below). Therefore, the properties assessed from regions near symmetry axes where the minimum image convention fails can be compared with those from regions near axes of the same symmetry but without imposed microscopic symmetry in the forces. In addition, the comparison is determined from one trajectory. This system is in contrast to the primary simulation unit being one asymmetric subunit, or the viral protomer equivalent of 1/60th of the icosahedron, for which symmetrical interactions would be imposed at all symmetry axes, and such a comparison would not be possible.

We show here from the analysis of a variety of physical properties that the imposed symmetry of forces has negligible influence on the resulting dynamics. An excluded volume for water molecules exists near axes with imposed symmetry; however this excluded volume did not perturb water structure or dynamics. Moreover, because protein atoms do not on average lie on a symmetry axis, no excluded volume effects were apparent in the simulation of HRV14. On the basis of the similarity in the dynamics and structural properties for regions with and without symmetry imposed in the forces, we conclude that RSBC simulations do not suffer from artifacts due to microscopic symmetry imposed near certain rotational axes, and RSBC is a reliable approach for reducing a simulation system with rotational symmetry.

2. METHODS

2.1. Computer Simulations. All molecular dynamics (MD) calculations were performed using the CHARMM program[11,12] with a constant volume and energy (NVE ensemble). A force switching function[13] was used to smoothly truncate electrostatic and van der Waals nonbonded forces at a cutoff of 14.0 Å. The covalent bonds to hydrogen atoms were constrained by the SHAKE algorithm. The equations of motion were integrated using the Verlet leapfrog algorithm with a time step of 1 fs. Icosahedral boundary conditions implemented with the IMAGES facility within CHARMM were employed as described below. Image atoms within 16.0 Å of a primary atom were included in the nonbonded pair list. Updates of image and nonbonded lists were made heuristically. All of the simulations were performed using a parallel version of CHARMM 35b2 running on a supercomputing cluster containing 893 eight-core Dell 1950 processors. Each simulation was performed on single node containing eight cores that shared 16 GB of RAM.

2.2. Rotational Symmetry Boundary Conditions. The simulation system for both bulk water and the solvated HRV14 capsid was an icosahedral shell rather than a solid icosahedron. Water molecules were constrained within the outer and inner radii by applying spherical quadratic potentials[14] referenced to 60 Å and 30 Å, respectively, for bulk water and 170 Å and 85 Å, respectively, for the solvated HRV14 capsid. The spherical quadratic potential was set up with a well depth of −0.25 kcal/mol at 1 Å from the reference distance followed by a smoothly rising repulsion. The lack of solvent in the central sphere of the icosahedron reduced the number of water molecules and avoided symmetrical interactions near the center.

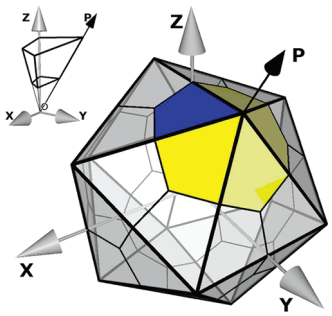

Figure 1. Schematic of an icosahedron with 20 triangular tiles. *O* is at the center of the icosahedron. Each tile has three asymmetric units corresponding to a protomer of the HRV14 capsid (blue area). The *Z* axis is coincident with one of the 2-fold symmetry axes. In this study, the pentamer, or five protomers centered around a 5-fold symmetry axis, is the primary unit cell (blue and yellow areas). The volume occupied by a protomer solvated in water, used in earlier studies,[6−8] is shown in the inset. Here, water molecules were removed from the center of the icosahedron, and a shell of water is used to solvate a protomer (thicker lines in the inset). Symmetry operators in the first row of Table 1 generate a solvated pentamer from the solvated protomer.

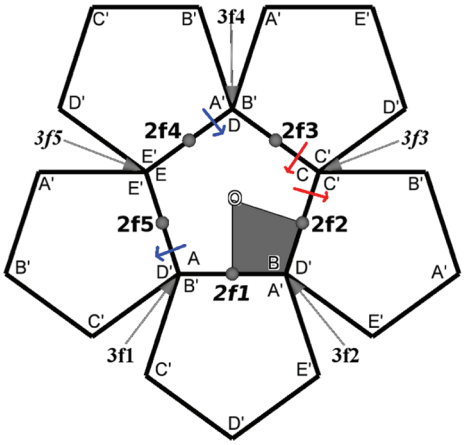

Figure 2. Two-dimensional projection of the pentamer and its neighbors generated by the set of symmetry operators shown in boldface in Table 1. The central pentamer represented by ABCDE, is the primary simulation unit. Pentamers represented by A′B′C′D′E′ are nearest-neighbor images. The area spanned by a protomer is represented by the shaded area. The 3-fold symmetry axes are 3f1 to *3f5*, and the 2-fold symmetry axes are *2f1* to 2f5. *O* is the 5-fold symmetry axis. The *Z* axis is coincident with *2f1*. Self-image and replicate-image interactions are present at one 2-fold symmetry axis, *2f1*, and two 3-fold symmetry axes, *3f3* and *3f5*.

The RSBC system was established from a subset of the 60 transformations for icosahedral symmetry listed in Table 1. The initial coordinates for the pentameric primary unit were generated by symmetry operations in the first row of Table 1 applied to a solvated HRV14 protomer (Figure 1, blue area). The solvated HRV14 protomer system, comprising four polypeptides (VP1, VP2, VP3, and VP4), was generated as described elsewhere.[6,7] Water molecules near the center of the icosahedron were removed to model an icosahedral shell. This primary unit for the HRV14 simulation system therefore comprises five protomer units around the 5-fold symmetry axis of icosahedron (Figure 1, blue and yellow areas). Coordinates for explicit atoms in the five nearest image

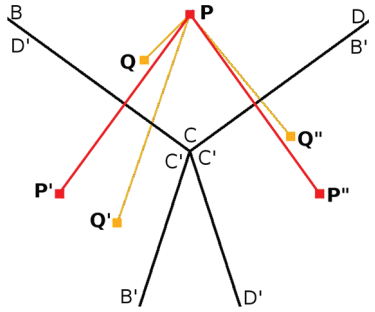

Figure 3. Illustration using the *3f3* axis of self-image and replicate-image interactions at a 3-fold symmetry axis of an icosahedron. BCD is part of the primary unit. B′C′D′ are images of BCD and produced by rotating BCD around a 3-fold symmetry axis. P and Q are two atoms in primary unit and P′,P″ and Q′,Q″ are their images, respectively. Minimum image convention is violated as Q, Q′, and Q″ are all within nonbonded interaction distance of P (replicate-image interaction). P also interacts with its own images P′ and P″ (self-image interaction). Microscopic symmetry is imposed on P as positions and velocities of P′ and P″, and Q′ and Q″ are solely determined by positions and velocities of P and Q, respectively.

units were generated by transformation of the primary atomic coordinates using the five rotational operators shown in boldface in Table 1. This selection of rotational symmetry operators from Table 1 uniquely satisfies the requirements for RSBC simulation. (See the Supporting Information for a detailed explanation of the selection of symmetry operators from Table 1.) The resulting simulation system of a pentameric primary unit and the five nearest-neighbor image units is shown projected in two dimensions in Figure 2. Recall that because the central pentamer is the primary unit, each corner, labeled A through E, is distinct from the other corners. As needed for periodic boundary conditions, the crossing of a boundary between the primary unit and an image unit is equivalent for all occurrences (illustrated by the blue or red arrows). These operators generate regions with imposed microscopic symmetry in the forces from self-image and replicate-image interactions near three symmetry axes (*2f1*, *3f3* and *3f5*), while regions around the remaining seven symmetry axes do not have such interactions. The axes with imposed symmetry are italicized through the paper to distinguish them from the other 2-fold and 3-fold axes. Self-image and replicate-image interactions are illustrated using the *3f3* axis in Figure 3. For the pure water simulation, a pentameric primary unit and image units were similarly generated from a spatial unit of bulk water analogous to the viral protomer.

2.3. Bulk Water Simulations and Analysis. A shell of TIP3 water, with an inner and outer radius of 30 Å and 60 Å, respectively, was modeled using a primary set of atoms corresponding to a pentameric shape with 2325 water molecules, and the five nearest image sets of atoms were generated using icosahedral symmetry operators as described above. Initial velocities were assigned randomly corresponding to 100 K, and the system was heated to 300 K over a time of 20 ps and then equilibrated for 180 ps. Velocities were reassigned during the equilibration period to maintain the target temperature. Analysis was done over the subsequent 800 ps trajectory period, during which the average temperature remained constant without velocity reassignment.

The oxygen−oxygen radial distribution function for water, $g(r)$, was computed using water molecules within a certain distance of a symmetry axis for the origin of integration. The $g(r)$ was determined for water molecules surrounding five 2-fold

symmetry axes, five 3-fold symmetry axes, one 5-fold symmetry axes of the icosahedral water shell, and an arbitrary axis through the spherical water shell from an MD simulation of TIP3 water calculated without RSBC. Two cutoff distances were used to select water molecules at the origin for $g(r)$ integration: 5 and 10 Å. The average number of water molecules within 5 Å was 28 near the 3-fold axes, 43 closest to the 2-fold axes, 86 near the 5-fold axis of the icosahedral water shell, and 86 near an arbitrary axis through the spherical shell of water. Histograms of bin width 0.1 Å were used to estimate $g(r)$.

To investigate whether the symmetrical forces imposed by RSBC affect the dynamical behavior of water molecules, we calculated the survival probability function,[15] $S_w(t)$, of water molecules in the vicinity of the axes of rotational symmetry. $S_w(t)$ gives the percentage of water molecules that remain in the vicinity of a symmetry axis after time t. To obtain $S_w(t)$, we compute the conditional probability $P_i(t_n,t)$ for each ith water molecule of the system. $P_i(t_n,t)$ takes a value of 1 if the ith water is in the vicinity of a symmetry axis between times t_n and $t_n + t$, and it has a value of zero otherwise. The survival probability is then

$$S_w(t) = \frac{100}{S_w(0)n_t}\sum_{n=1}^{n_t}\sum_i P_i(t_n,t) \quad (2)$$

Here, n_t is the number of simulation time-frames, and $S_w(0)$ is the average number of water molecules in the vicinity of a symmetry axis. If the oxygen atom of a water molecule is within a certain radial distance of a symmetry axis, we consider the water molecule to be within the vicinity of that symmetry axis. Image atoms were also considered while counting water molecules. With the choice of symmetry operators indicated by Figure 2, the symmetry axes 3f1, 3f2, and 3f4 correspond to equivalent regions (A, B, and D) and will therefore will have same density of water. The microenvironment and hence the number of water molecules near the 3-fold symmetry axis 3f1 will be exactly that near 3f2 and 3f4. Similarly, the count near 2-fold symmetry axis 2f2 will be exactly that near 2f3, and 2f4 will be exactly that near 2f5.

We used an orientational order parameter (Q)[16] to investigate the structure of water.

$$Q \equiv 1 - \frac{3}{8}\sum_{j=1}^{3}\sum_{k=j+1}^{4}\left(\cos\psi_{jk} + \frac{1}{3}\right)^2 \quad (3)$$

where ψ_{jk} is the angle formed by the lines joining the oxygen atom of a given water molecule and those of nearest neighbors j and k. For the purpose of this study, we limit our attention to the four oxygen atoms nearest a given oxygen atom. Here, Q is slightly modified from previous work[17] to have the value $\langle Q\rangle = 0$ ($\langle ...\rangle$ denotes the ensemble average) in the ideal gas phase[16] and $Q = 1$ for a perfect tetrahedral configuration. Thus, Q measures the degree of tetrahedrality in the distribution of the four nearest oxygen atoms around a central oxygen atom.

We considered effects on the instantaneous temperature, which depends on the root-mean-square speed, (V_{rms}).

$$V_{rms} \equiv \sqrt{\frac{\sum_{i=1}^{n} m_i v_i^2}{\sum_{i=1}^{n} m_i}} \quad (4)$$

where n is number of atoms and m_i and v_i are the mass and magnitude of velocity of the ith atom.

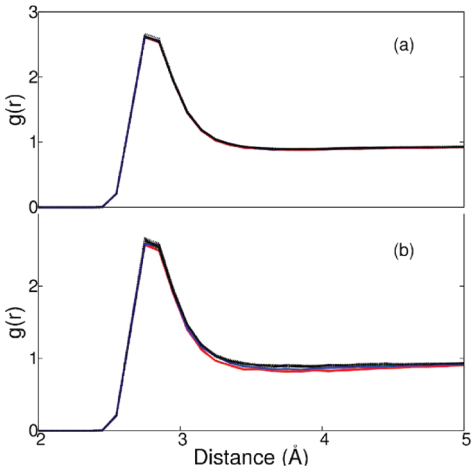

Figure 4. Radial distribution function of O−O distances for water molecules within (a) 10 Å or (b) 5 Å of *3f3* and *3f5* (red); *2f1* (blue); other 2-fold, 3-fold, and 5-fold symmetry axes of the icosahedron shell of water; and an arbitrary axis through the spherical shell of water (black).

2.4. Solvated HRV14 Capsid Simulations. Coordinates of the HRV14 protomer (protein data bank: 4RHV[18]) were used to generate the pentamer composing the primary set of atoms with the operators of row 1, Table 1 as described above. Missing virus coordinates were modeled on the basis of homologous residues in human rhinovirus 16 (protein data bank: 1AYM[19]) or polio virus (protein data bank: 1HXS[20]). The energy of the modeled residues was minimized while maintaining the known HRV14 crystallographic coordinates at a fixed value. Keeping the known atomic positions fixed, in a vacuum, NVE MD simulations were performed to raise the temperature of the modeled regions over a 490 ps period from 100 to 5000 K; the system was annealed at 5000 K for a 50 ps period and then cooled to 300 K over a 980 ps period.

Electron density at the 3-fold and 5-fold symmetry axes has been interpreted to be a calcium ion.[21] Following simulated annealing, one calcium ion was therefore placed at the crystallographic position on a 5-fold symmetry axis and 3-fold symmetry axis 3f1 in Figure 2. Symmetry operations generated images of a calcium ion on 3f2 and 3f4 from a calcium ion on 3f1. Modified calcium ions, with one-third of the charge and the mass of a calcium ion as described elsewhere,[6] were placed at their crystallographic position on the 3-fold symmetry axes *3f3* and *3f5*. The HRV14 pentamer with calcium ions was solvated following a known protocol. The charge of the solvated pentamer was neutralized by randomly replacing the appropriate number of water molecules with counterions, and the interior and exterior of the viral capsid were neutralized independently. The energy of the final primary unit, comprising 25 596 water molecules and a total of 142 456 atoms, was minimized using the protocol described elsewhere.[6] Velocities corresponding to 100 K were assigned randomly to the charge neutralized viral capsid and heated to 300 K over a time of 20 ps. The solvated capsid was then allowed to equilibrate over a 980 ps period. A further 2 ns period of MD simulation was performed for analysis. Properties investigated in this article depend on the magnitude of atomic velocities, the density of atoms within a shell of different thickness near a symmetry axis, and the distribution of ϕ and ψ dihedral angles. All of these values were well converged during the 2 ns MD production period (see the Supporting Information).

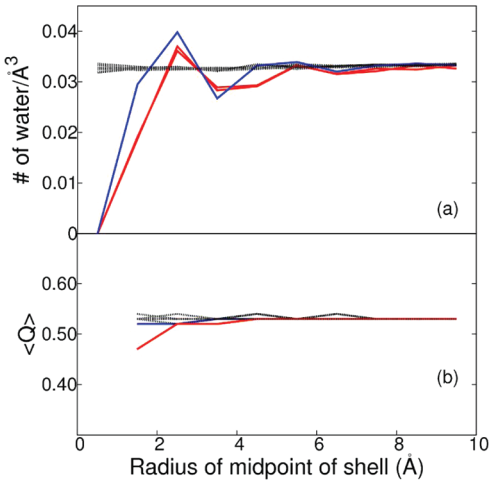

Figure 5. Density and orientational order parameter, Q, of water within cylindrical shells of 1 Å width around the *3f3* and *3f5* (red); 2f1 (*blue*); other 2-fold, 3-fold, and 5-fold symmetry axes of the icosahedron shell of water; and an arbitrary axis through the spherical shell of water (black). (a) The density of water at X Å is calculated from the average number of water molecules between $X - 0.5$ Å and $X + 0.5$ Å over the simulation time period for X from 0.5 to 9.5 Å in 1 Å intervals. (b) $\langle Q \rangle$ within a cylindrical shell of 1 Å width is calculated by averaging the Q of individual waters within the shell over the simulation time period.

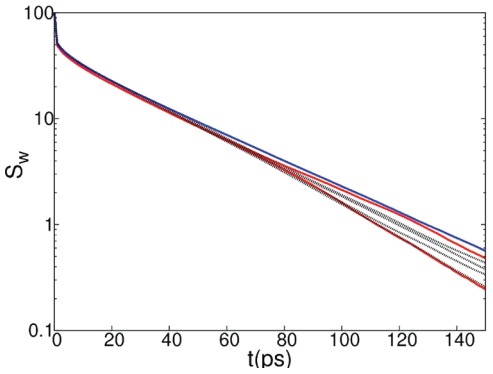

Figure 6. Survival probabilities of water molecules within 10 Å of *3f3* and *3f5* (red); *2f1* (blue); and other 2-fold, 3-fold, and 5-fold symmetry axes (black) from the simulation of an icosahedron shell of water.

3. RESULTS AND DISCUSSION

3.1. Bulk Water. A shell of bulk water was simulated under RSBC using TIP3 water. Icosahedral symmetry restraints were set up as shown in Figure 2 with the primary unit equivalent to an icosahedral pentamer and the surrounding five replicated image units. Explicit image atoms were generated according to the operators shown in Figure 2. Symmetry is imposed on the forces from self-image and replicate-image interactions that occur near the axes *2f1*, *3f3*, and *3f5*. Interactions at the other 2-fold and 3-fold axes are uniquely determined and without imposed symmetry. Potential effects due to the nonphysical microscopic symmetry imposed *2f1*, *3f3*, and *3f5* in RSBC MD simulations of bulk water were assessed by comparing structural and dynamic properties evaluated from water molecules near these symmetry axes with the same properties evaluated near other icosahedral symmetry axes.

3.1.1. Influence on Structural Properties. The $g(r)$ functions are plotted for averages over water molecules within 10 Å (Figure 4a) or 5 Å (Figure 4b) of a symmetry axis. The plots in Figure 4a are indistinguishable for distributions within 10 Å of any of the 12 axes, including those with imposed microscopic symmetry. Considering distributions for water molecules positioned within 5 Å of an axis, $g(r)$ is only somewhat perturbed by the imposed symmetry. Between 3 and 5 Å, the density is slightly lower for regions near *2f1* (blue) and *3f3* and *3f5* (red) than regions near the other symmetry axes (Figure 4b).

An inevitable consequence of the imposed symmetry surrounding the *2f1*, *3f3*, and *3f5* axes is that an atom cannot occupy this region in space due to steric collision with its own image. As a result, an excluded volume of cylindrical shape surrounds *2f1*, *3f3*, and *3f5* in the simulation system. The excluded volume was characterized by determining the water density in 1-Å-thick cylindrical shells from 0.5 to 9.5 Å radii, in 1 Å increments, around each of the 2-fold, 3-fold, and 5-fold symmetry axes of the RSBC simulation of a water shell and around an arbitrary axis for the spherical water shell simulation. The coordinate of the water oxygen was used to specify occupancy. The water density averaged over the simulation time period is plotted as a function of the cylindrical radius in Figure 5a for each of the 12 axes defined in the Methods section. There is no water molecule within 1 Å of the *2f1*, *3f3*, or *3f5* axis. The radius of the excluded cylindrical volume is between 1 and 2 Å and is slightly larger for the 3-fold symmetry axes than the 2-fold symmetry axis. The total excluded volume is about 0.01% of the icosahedral pentameric water shell. The excluded volume at the *2f1*, *3f3*, and *3f5* axes is compensated by increased density between 2 and 3 Å of those symmetry axes, so that beyond 6−7 Å (less than the dimension of two water molecules), the density of water at *2f1*, *3f3*, and *3f5* is unperturbed relative to that of bulk water and that near the other symmetry axes.

To examine whether the excluded volume and variation in water density (Figure 5a) affected the water structure in the vicinity of these symmetry axes, we examined the value of Q (see the Methods section). The ensemble averaged values $\langle Q \rangle$ for water molecules within cylindrical shells of varying radii are shown in Figure 5b. $\langle Q \rangle$ is between 0.52 and 0.53 for water molecules near all symmetry axes except those close to *3f3* and *3f5*. The value for $\langle Q \rangle$ is 0.47 for averaging over water molecules within 2 Å of *3f3* and *3f5* but reaches 0.52 for averaging waters at a distance greater than 2 Å from those axes. Thus, only the first layer of water near *3f3* and *3f5* deviates slightly from the tetrahedrality of bulk water measured by Q.

3.1.2. Influence on Dynamical Properties. To investigate whether the symmetry imposed by RSBC affects the dynamical behavior of water molecules, we calculated the survival probability, $S_w(t)$, of water within 10 Å of symmetry axes (Figure 6).

The differences in the $S_w(t)$ of water, near the *2f1*, *3f3*, or *3f5* axes relative to that for the other symmetry axes, are not greater than the differences among the other symmetry axes. The spread in curves in Figure 6 at 150 ps is less than one water molecule, and there is no clear trend in the spread that would indicate water molecules reside for longer or shorter times near the *2f1*, *3f3*, or *3f5* axes compared to the other symmetry axes. Even though the density of water is lower near the *2f1*, *3f3*, and *3f5* axes, the survival probability of water is not changed near these symmetry axes.

A comparison of the fluctuations in instantaneous temperature for the water molecules near the *2f1*, *3f3*, and *3f5* axes with symmetry imposed in nonbonded forces to the fluctuations for the rest of the system should also indicate potential artifacts in

Table 2. Root Mean Square Speed (V_{rms}) and Flux of Water[a]

	V_{rms} Å/ps	δV_{rms} Å/ps	$\Phi(S_1)$ 1/ps/Å^2	$\delta\Phi(S_1)$ 1/ps/Å^2	$\Phi(S_2)$ 1/ps/Å^2	$\delta\Phi(S_2)$ 1/ps/Å^2
2f1	0.32	0.02	0.00	0.02		
2f2,2f3,2f4,2f5	0.32	0.02	0.00	0.02		
3f3	0.32	0.03	0.00	0.02	0.00	0.02
3f5	0.32	0.02	0.00	0.02	0.00	0.02
3f1,3f2,3f4	0.32	0.02	0.00	0.02	0.00	0.02

[a] Root mean square speed (V_{rms}) and their fluctuations (δV_{rms}); flux through adjacent surfaces (Φ) and their fluctuations ($\delta\Phi$) of water molecules within 5 Å of a symmetry axes. For a 3-fold symmetry axis, the flux through two individual adjacent surfaces (S_1, S_2) of the primary unit edge was determined. For a 2-fold symmetry axis, the flux through the primary unit surface (S_1) containing the symmetry axis was determined.

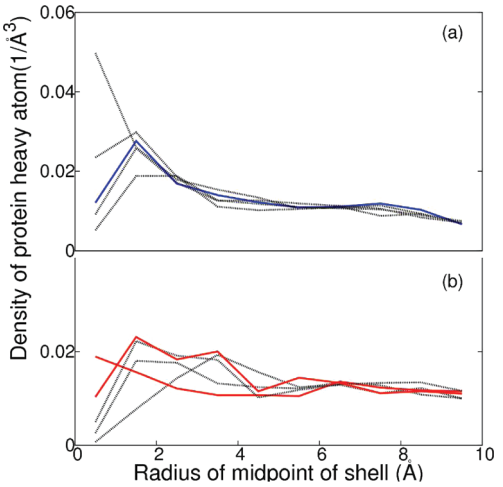

Figure 7. Density of protein within a cylindrical shell of 1 Å width around (a) 2-fold symmetry axes (*2f1*, blue) and other 2-fold symmetry axes (black) and (*b*) 3-fold symmetry axes *3f3* and *3f5* (red) and other 3-fold symmetry axes (black). The density of water at *X* Å is calculated by calculating the average density of protein atoms between $X - 0.5$ Å and $X + 0.5$ Å over the simulation time period. The density was calculated for *X* from 0.5 Å to 9.5 Å in 1 Å intervals.

the dynamical behavior of water. Fluctuations in temperature arise from fluctuations in magnitude of atomic velocities, δV_{rms}. The δV_{rms} values for water molecules in a cylinder of 5 Å radius around symmetry axes listed in Table 2 are nearly equivalent, indicating no differences in fluctuation of instantaneous temperature.

The flux, Φ, through two adjacent surfaces of the primary unit defining the corner near the 3-fold symmetry axes and the surface of the primary unit containing the 2-fold symmetry axes was also calculated. The flux does not diverge near *2f1*, *3f3*, and *3f5*, as no net flux of water molecules was observed through the adjacent surfaces of those three symmetry axes (Table 2).

Overall, the results from MD simulation of bulk water including RSBC indicate that the symmetrical force from self-image interactions and other replicate-image nonbonded interactions imposed by an axis of rotational symmetry do not give rise to artifacts other than the presence of an excluded volume of radius between 1 and 2 Å at the symmetry axes, which alters the density of no more than two water layers. RSBC changes the structure of the first water layer somewhat near the region of excluded volume, but no differences were observed in the dynamical behavior of water molecules near these rotational axes.

3.2. HRV14 Capsid. As an asymmetric molecule, the protein atoms approach an axis of rotational symmetry but, on average, cannot lie on an axis. In the energy-minimized crystal structure,

Table 3. Root Mean Square Speed (V_{rms}) of Protein[a]

3-fold symmetry axes	V_{rms} Å/ps	δV_{rms} Å/ps
3f1	0.37	0.06
3f2	0.37	0.06
3f3	0.38	0.06
3f4	0.38	0.06
3f5	0.37	0.06

[a] Root mean square speed (V_{rms}) and fluctuations (δV_{rms}) of residue 117 of VP2 near five 3-fold symmetry axes. Interactions near the symmetry axes *3f3* and *3f5* violate the minimum image convention.

the closest heavy-atom distance to a 3-fold symmetry axis is 2.5 Å, and 2.8 Å on average, while the distance to a 2-fold axis is 1.1 Å, and 1.6 Å on average. In further contrast to water molecules, given the mass and covalent structure, protein atoms do not experience overall translational motion and reorientation within the simulation boundaries. Accordingly, the protein structure and dynamics would seem less susceptible to the influence of imposed symmetry from RSBC, and effects such as the excluded volume apparent for water molecules would be diminished for a protein molecule.

The density of HRV14 atoms was determined as a function of the radial distance from the axes of rotational symmetry in the fashion outlined above for water molecules. Densities of HRV14 heavy atoms within cylindrical shells 1-Å-thick around the 2-fold and 3-fold symmetry axes are shown in Figure 7a and b, respectively. The variation among the density profiles for all of the axes is as large between those without symmetry imposed as it is between those with and without symmetry imposed, and no trend in the profiles distinguishes the density of the protein atoms surrounding the *2f1*, *3f3*, and *3f5* axes from that surrounding the other axes. The profile around one of the 2-fold axes exhibits an interesting increase at short distance, which shows a microscopic breakdown of symmetry due to a conformational fluctuation that moves the protein toward the region of the symmetry axes. Although this type of fluctuation would be less probable at the *2f1* axis, the overall behavior shown in Figure 7 shows no differences from RSBC.

If the self-image interactions of the protein molecule near *2f1*, *3f3* and *3f5* generate artificial forces, fluctuation of instantaneous temperature of the protein residues near those axes should increase. We examined the V_{rms} of residue 117 of VP2, which is nearest to the 3-fold symmetry axes. Fluctuation of V_{rms} for VP2 117 from each of the five protomers in the pentameric set of primary atoms shown in Table 3 and indicate no significant differences in trend for VP2 117 near the *3f3*, *3f5* or other 3-fold symmetry axes.

We also examined structural features of residues near the five 3-fold axes. The distribution of the main chain ϕ,ψ dihedral

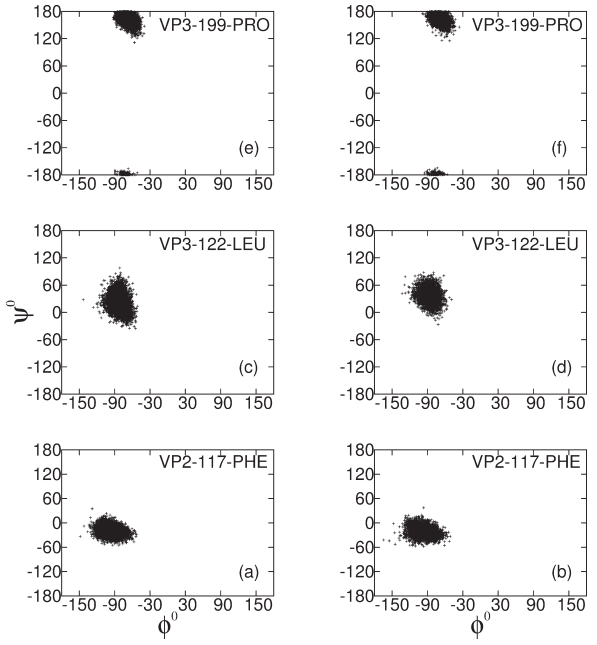

Figure 8. Ramachandran plot of residues closest to 3-fold symmetry axes. The dihedral angles, ϕ and ψ, are plotted for residue 117 of VP2 and residues 122 and 199 of VP3 from protomers located near the 3f1, 3f2, and 3f4 axes (Figure 8a, c, and e) or located near the *3f3* and *3f5* axes (Figure 8b, d, and f).

angles are shown for the residues 117 of VP2 and 122 and 199 of VP3 in Figure 8. These Ramachandran plots reveal that the distributions for these residues positioned near the 3f1, 3f2, or 3f4 axes (Figure 8a, c, and e) do not differ from those at the *3f3* or *3f5* axes (Figure 8b, d, and f), and thus the protein main-chain conformation is not effected by self-image interactions.

Together these results show that neither the structural nor dynamical behavior of the HRV viral capsid is perturbed by self-image or replicate-image interactions imposed by RSBC. The excluded volume effect, demonstrated by the density profile from bulk water simulation (Figure 5), is not manifested by the protein atoms. The fact that protein atoms, on average, cannot lie on a symmetry axis reduces the potential for artifacts induced by RSBC, and the inherent excluded volume poses practically no problem.

4. CONCLUSION

In this article, we have studied in depth the effect of the nonphysical microscopic symmetry imposed by RSBC on MD simulations of an icosahedral shell of bulk water and HRV14 viral capsid and examined the effect due to symmetry imposed at certain axes based on the similarity of properties that are well converged in the 2 ns simulation period. The approach is a reasonable critical assessment of the resulting forces and dynamics even though longer time scale properties may not be fully converged in the 2 ns simulation. Selection of the primary unit to correspond to five protomers of this virus allowed comparisons within a single trajectory of structural and dynamic properties at rotational axes with and without imposed symmetries. The only significant difference observed is the density of water within 6 Å of a rotational symmetry axis with imposed microscopic symmetry (Figure 5a). This excluded volume is unavoidable given the nonphysical nonbonded interactions to self-images. Nevertheless, the structural and dynamical behavior of water remains without perturbation.

No differences in dynamics or structure due to the volume excluded by self-images were observed for the large protein system of HRV14. As a result of the many contributions to the atomic forces of the system, protein atoms can fluctuate into regions within 1 Å of a symmetry axis where self-image interactions occur (red line in Figure 7b). The sub-Ångstrom excluded volume due to self-image interaction affected neither the dynamics nor the structural properties of the viral protein.

In summary, we have validated the usage of RSBC to minimize the size of a system with rotational symmetry. Usage of a pentamer as the primary unit can minimize the artifacts by avoiding the higher symmetry surrounding the 5-fold axis. While a pentamer as the primary unit will only reduce the size of the system by about 12-fold instead of 60-fold if a protomer were chosen as a primary unit, a pentamer of a viral capsid, with about 65 000 atoms and 26 000 water molecules, is well within the capacity of simulation using modern day computers.

■ ASSOCIATED CONTENT

Supporting Information. A detailed discussion of the implementation of RSBC, an explanation of minimum image violation at certain symmetry axes, and a discussion on convergence of properties investigated in the article. This material is available free of charge via the Internet at http://pubs.acs.org/.

■ AUTHOR INFORMATION

Corresponding Author

*E-mail: cbp@purdue.edu.

Funding Sources

This work was supported by the National Institutes of Health (grant no. AI039639)

■ ACKNOWLEDGMENT

We thank Rosen Center for Advanced Computing at Purdue University for providing computing resources. We thank He Huang and Joshua Ward for meaningful discussions about symmetry operators of the reduced icosahedral group and early setup of MD simulations.

■ REFERENCES

(1) Tama, F.; Brooks, C., III. *J. Mol. Biol.* **2005**, *345*, 299–314.
(2) Vaidehi, N.; Goddard, W. A., III. *Proc. Natl. Acad. Sci. U.S.A.* **1997**, *94*, 2466–2471.
(3) Zink, M.; Grubmüller, H. *Biophys. J.* **2010**, *98*, 687–695.
(4) Zink, M.; Grubmüller, H. *Biophys. J.* **2009**, *96*, 1350–1363.
(5) Cagin, T.; Holder, M.; Pettitt, B. M. *J. Comput. Chem.* **1991**, *12*, 627–634.
(6) Speelman, B.; Brooks, B.; Post, C. B. *Biophys. J.* **2001**, *80*, 121–129.
(7) Li, Y.; Zhou, Z.; Post, C. B. *Proc. Natl. Acad. Sci. U.S.A.* **2005**, *102*, 7529–7534.
(8) Yoneda, S.; Kitazawa, M.; Umeyama, H. *J. Comput. Chem.* **1996**, *17*, 191–203.
(9) Milne, J. L. S.; Shi, D.; Rosenthal, P. B.; Sunshine, J. S.; Domingo, G. J.; Wu, X.; Brooks, B. R.; Perham, R. N.; Henderson, R.; Subramaniam, S. *EMBO J.* **2002**, *21*, 5587–5598.
(10) Blundell, T. L.; Srinivasan, N. *Proc. Natl. Acad. Sci. U.S.A.* **1996**, *93*, 14243–14248.

(11) Brooks, B. R.; Bruccoleri, R. E.; Olafson, B. D.; States, D. J.; Swaminathan, S.; Karplus, M. *J. Comput. Chem.* **1983**, *4*, 187–217.
(12) Brooks, B. R.; Brooks, C. L., III; Mackerell, A. D., Jr; Nilsson, L.; Petrella, R. J.; Roux, B.; Won, Y.; Archontis, G.; Bartels, C.; Boresch, S.; Caflisch, A.; Caves, L.; Cui, Q.; Dinner, A. R.; Feig, M.; Fischer, S.; Gao, J.; Hodoscek, M.; Im, W.; Kuczera, K.; Lazaridis, T.; Ma, J.; Ovchinnikov, V.; Paci, E.; Pastor, R. W.; Post, C. B.; Pu, J. Z.; Schaefer, M.; Tidor, B.; Venable, R. M.; Woodcock, H. L.; Wu, X.; Yang, W.; York, D. M.; Karplus, M. *J. Comput. Chem.* **2009**, *30*, 1545–1614.
(13) Steinbach, P. J.; Brooks, B. R. *J. Comput. Chem.* **1994**, *15*, 667–683.
(14) CHARMM:mmfp.doc. http://www.charmm.org/documentation/c35b1/mmfp.html (accessed July 26,2011).
(15) Pizzituttu, F.; Marchi, M.; Rossky, P. J.; Sterpone, F. *J. Phys. Chem. B* **2007**, *111*, 7584–7590.
(16) Chau, P. L.; Hardwick, A. J. *Mol. Phys.* **1998**, *93*, 511–518.
(17) Giovambattista, N.; Debenedetti, P. G.; Sciortino, F.; Stanley, H. E. *Phys. Rev. E* **2005**, *71*, 061505–061512.
(18) Rossmann, M. G.; Arnold, E.; Erickson, J. W.; Frankenberger, E. A.; Griffith, J. P.; Hecht, H. J.; Johnson, J. E.; Kamer, G.; Luo, M.; Mosser, A. G.; Rueckert, R. R.; Sherry, B.; Vriend, G. *Nature* **1985**, *317*, 145–153.
(19) Hadfield, A. T.; Lee, W.; Zhao, R.; Oliviera, M. A.; Minor, I.; Rueckert, R. R.; Rossmann, M. G. *Structure* **1997**, *5*, 427–441.
(20) Miller, S. T.; Hogle, J. M.; Filman, D. J. *J. Mol. Biol.* **2001**, *307*, 499–512.
(21) Zhao, R.; Hadfield, A. T.; Kremer, M. J.; Rossmann, M. G. *Virology* **1997**, *227*, 13–23.

Supporting information for: Microscopic Symmetry Imposed by Rotational Symmetry Boundary Conditions in Molecular Dynamics Simulation

Amitava Roy and Carol Beth Post*

E-mail: cbp@purdue.edu

1 Rotational Symmetry Boundary Condition (RSBC)

Periodicity treated implicitly determines nonbonded interaction using the minimum image convention:

$$\acute{V_a} = V_a - nearint[V_a/L_a] \cdot L_a, \tag{1}$$

where V_a and $\acute{V_a}$ are component of distance vectors, L_a is the length of the periodic box along V_a, and $nearint[...]$ is nearest integer value of $[...]$. Application of Eq. (1) to relative distances in an infinite periodic system allows selection of the closest copy of replicated atoms for determining the nonbonded interactions in open crystallographic space group symmetry. Self-image interactions are avoided with an appropriate sized primary unit. With closed point group symmetry and rotational symmetry boundary conditions (RSBC), it is not possible to utilize the minimum image convention or to avoid self-image and replicate-image interactions near certain rotational symmetry axes. A subset of the 60 icosahedral symmetry operators is needed to generate the full capsid from a pentameric primary unit. The choice of the subset can be optimized to minimize, but not avoid, the self-image and replicate-image interactions.

*To whom correspondence should be addressed

The choice for the subset of icosahedral symmetry operators must meet two criteria:[1]

1. In explicit treatment of image atoms, when primary atoms cross a wall of the primary cell, their coordinates are transformed back into the primary cell using inverse of one of the image operators. This procedure is called re-centering. To avoid a discontinuity in energy, re-centering must move the atom to the identical micro-environment, with equivalent nonbonded interactions for primary and image atoms as existed before re-centering. Re-centering is essential for implementation of a general symmetry boundary condition because of the explicit treatment of image atoms. Without re-centering, water molecules that leave the primary cell will interact with an increasing number of image atoms leading to a corresponding increase in the nonbonded pair list. As a result, the total energy of the system decreases over time (data not shown here).

2. Each symmetry operator must have its inverse operator in the listed subset of operators. This requirement of the IMAGE facility of CHARMM is imposed for computational efficiency in calculating energies.[2] Fulfillment of the first criterion guarantees fulfillment of this criterion for the subset of icosahedral symmetry operators used in this article.

A subset of the icosahedral symmetry operators (Table 1) was selected to transform the primary coordinates to image coordinates. For the five nearest neighbor units positioned at the pentamer edges of the primary unit the symmetry operators were selected such that symmetrical forces were imposed at some but not all rotational axes. The five operators of each row of Table 1 transform an asymmetric unit, or protomer of a virus, to a pentameric unit. Assuming the top-row operators form the pentamer of the primary unit, one operator of each row 2-12 is needed to complete an icosahedron. We limit our attention to generating images of only neighboring pentamers given that the pentamer size is greater than the nonbonded cutoff distance. Operators in bold face in rows 2, 5, 6, 9, and 11 of Table 1 generate these neighboring pentamers. The only set of operators, one from each of these rows, that satisfies the two conditions for the IMAGE facility enumerated above are the operators Z (row 2), F_1ZF_3 (row 5), ZF_1ZF_3 (row 6), F_2ZF_4 (row 9), and XF_2ZF_4

(row 11). The set contains the inverse of each operator; the Z transformation is self-inverse, while F_1ZF_3/F_2ZF_4 and ZF_1ZF_3/XF_2ZF_4 are inverse transformations. That the first condition is satisfied can be determined from Figure 1a, which shows in a two-dimensional projection the primary unit and five nearest-neighbor image units generated with this choice of icosahedral operators. Recall that, because the pentamer is the primary simulation set, each pentameric corner, labeled A through E, is distinct from the other corners. An atom leaving primary unit near 3f1, as shown in Figure 1a, will be re-centered near 3f4. Before leaving the primary unit atom was interacting with primary atoms near corner A and images of atoms near corner B and D. After re-centering the atom will interact with primary atoms near corner D and images of atoms near corner A and B. Thus re-centering of atoms that move into an image region returns the atom to the exact environment within the primary unit. Similarly an atom near 3f3 leaving primary unit will be re-centered near 3f3. Figure 1b show two-dimensional projection of primary unit and five nearest-neighbor image units generated with symmetry operators underlined in Table 1 which do not satisfy the first criterion mentioned above. An atom leaving primary unit near 3f1 in Figure 1b, where micro-environment generated by corners A, B & E, will be re-centered near 3f2 where the micro-environment is different and generated by corners A, B & D. Simulation can not be performed with such a set of symmetry operators as energy will be discontinuous after re-centering.

Figure 1a showing the primary pentameric unit of the icosahedron and illustrates the failure at certain axes of rotational symmetry of the minimum image convention used for generating non-bonded list under periodic boundary conditions. Clearly this algorithm fails near axes *2f1*, *3f3* and *3f5* as explained in section 2.2 of article. Near other symmetry axes images are not positioned near the primary unit guarantees avoidance of replicate-image and self-image interactions. For example near axes 3f1 of Figure 1a atoms near $\angle EAB$ interacts with atoms near $\angle C'D'E'$ and $\angle A'B'C'$ of image units and avoid self-image and replicate-image interactions. In spite of violations of minimum image convention near certain symmetry axes, RSBC are properly handled by explicit treatment of image atoms with the limitation that the resulting interactions impose microscopic symmetry of forces for a small number of nonbonded pairs.

At the 2-fold symmetry axis *2f1*, and 3-fold symmetry axes *3f3* and *3f5* (Figure 1a) microscopic symmetry is imposed by forces from self-image interactions and from interactions with replicate primary and image atoms located near the axes. Other 2-fold, 3-fold, and of course, the 5-fold icosahedral symmetry axes are microscopically asymmetric given that primary and image atoms are not replicated and all nonbonded interactions are with independent atoms.

2 Convergence

Properties investigated in this article depend on magnitude of V_{rms} and the density of atoms within a shell of different thickness near a symmetry axis.

$$V_{rms} \equiv \sqrt{\frac{\sum_{i=1}^{n} m_i v_i^2}{\sum_{i=1}^{n} m_i}} \tag{2}$$

where n is number of atoms and m_i and v_i are mass and magnitude of velocity of ith atom.

Instantaneous temperature the system depends on V_{rms}.

$$T(t) = \sum_{i=1}^{N} \frac{m_i v_i^2(t)}{k_B N_f} \tag{3}$$

where N is total number of atom in the system, N_f id number of degrees of freedom and k_B is Boltzmann's constant.

In Figure 2a temperature of solvated viral capsid during 2 ns production time of simulation is shown. Densities of heavy atoms of viral capsid within cylindrical shells of 1 Å width around 3-fold symmetry axis 3f1 are shown in Figure 2b. Densities are shown for shell at 3 different distances with their midpoints at 5 Å (red), 7 Å (green) and 9 Å (blue). Both temperature and densities of heavy atom are well converged during the simulation.

In Figure 3 the distribution of the main chain ϕ, ψ dihedral angles are shown for the residues 117 of VP2, and 122 and 199 of VP3 in Figure 3 for four additional sets of 2 ns production time of simulation. These Ramachandran plots reveal that the distributions for these residues positioned

near the 3f1, 3f2 or 3f4 axes (panel a,c and e in Figure 3) do not differ from those at *3f3* or *3f5* axes (panel b,d and f in Figure 3). In 5 different independent simulations the ϕ, ψ dihedral angles spans similar area in Ramachandran plots which indicates that in 2 ns of production time lowest energy regions of underlying energy surface are well populated.

References

(1) Brooks B.R., C.L. Brooks 3rd, A.D. Mackerell Jr, L. Nilsson, R.J. Petrella, B. Roux, Y. Won, G. Archontis, C. Bartels, S. Boresch, A. Caflisch, L. Caves, Q. Cui, A.R. Dinner, M. Feig, S. Fischer, J. Gao, M. Hodoscek, W. Im, K. Kuczera, T. Lazaridis, J. Ma, V. Ovchinnikov, E. Paci, R.W. Pastor, C.B. Post, J.Z. Pu, M. Schaefer, B. Tidor, R.M. Venable, H.L. Woodcock, X. Wu, W. Yang, D.M. York, and M. Karplus *J. Comput. Chem.*, **30, 2009**, 1545–1614.

(2) R. Brooks B., R. E. Bruccoleri, B. D. Olafson, D. J. States, S. Swaminathan, and M. Karplus. *J. Comput. Chem.*, **4, 1983**, 187–217.

(3) Frenkel D, Smit B *Understanding Molecular Simulation* Academic Press: New York **2002**, 64–65.

Table 1: **Icosahedral symmetry operators**[a]

	1	2	3	4	5
1	I (1,1)	F_1 (1,5)	F_2 (1,4)	F_3 (1,3)	F_4 (1,2)
2	**Z** (2,1)	ZF_1 (6,2)	$\underline{ZF_2}$ (11,4)	ZF_3 (9,1)	ZF_4 (5,1)
3	X (3,1)	XF_1 (8,1)	$\overline{XF_2}$ (12,1)	XF_3 (10,4)	XF_4 (7,2)
4	Y (4,1)	YF_1 (4,2)	YF_2 (4,3)	YF_3 (4,4)	YF_4 (4,5)
5	F_1Z (2,5)	$\underline{F_1ZF_1}$ (6,1)	F_1ZF_2 (11,3)	$\mathbf{F_1ZF_3}$ (9,5)	F_1ZF_4 (5,5)
6	$\underline{ZF_1Z}$ (5,2)	$\overline{ZF_1ZF_1}$ (2,2)	ZF_1ZF_2 (6,3)	$\mathbf{ZF_1ZF_3}$ (11,5)	ZF_1ZF_4 (9,2)
7	$\overline{XF_1Z}$ (7,1)	XF_1ZF_1 (3,5)	XF_1ZF_2 (8,5)	XF_1ZF_3 (12,5)	XF_1ZF_4 (10,3)
8	YF_1Z (3,2)	YF_1ZF_1 (8,2)	YF_1ZF_2 (12,2)	YF_1ZF_3 (10,5)	YF_1ZF_4 (7,3)
9	F_2Z (2,4)	F_2ZF_1 (6,5)	F_2ZF_2 (11,2)	$\underline{F_2ZF_3}$ (9,4)	$\mathbf{F_2ZF_4}$ (5,4)
10	ZF_2Z (12,4)	ZF_2ZF_1 (10,2)	ZF_2ZF_2 (7,5)	$\overline{ZF_2ZF_3}$ (3,4)	ZF_2ZF_4 (8,4)
11	XF_2Z (11,1)	XF_2ZF_1 (9,3)	XF_2ZF_2 (5,3)	$\underline{XF_2ZF_3}$ (2,3)	$\mathbf{XF_2ZF_4}$ (6,4)
12	YF_2Z (3,3)	YF_2ZF_1 (8,3)	YF_2ZF_2 (12,3)	$\overline{YF_2ZF_3}$ (10,1)	YF_2ZF_4 (7,4)

[a] Rotational operators of icosahedral symmetry. I is identity; $F_{1,2,3,4}$ are rotations around the 5 fold symmetry axis by 72^0, 144^0, 216^0, 288^0 respectively; X,Y,Z are rotations by 180^0 around X,Y,Z axes respectively. The 1st and 2nd numbers inside the parenthesis following the operator indicates the row and column numbers respectively of the inverse of that operator. Five operators in each row transform the protomer coordinates to 5 protomers for the pentameric primary unit used in this study. Neighboring images of the pentameric unit are generated by the five operators in boldface.

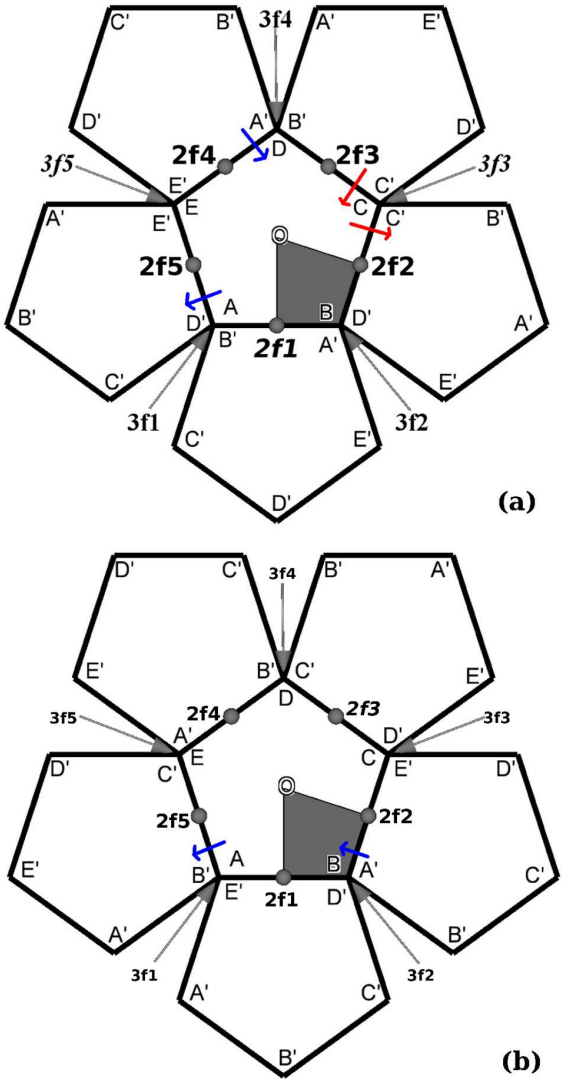

Figure 1: (a) Two-dimensional projection of the pentamer and its neighbors generated by the set of symmetry operators shown in bold face in Table 1. The central pentamer represented by *ABCDE*, is the primary simulation unit. Pentamers represented by $A'B'C'D'E'$ are nearest-neighbor images. The area spanned by a protomer is represented by the shaded area. Three-fold symmetry axes are 3f1 to *3f5* and two-fold symmetry axes are *2f1* to 2f5. *O* is the five-fold symmetry axis. The Z axis is coincident with *2f1*. Self-image and replicate-image interactions are present at one 2-fold symmetry axis, *2f1*, and two 3-fold symmetry axes, *3f3* and *3f5*. (b) Two-dimensional projection of the pentamer and its neighbors generated by the set of underlined symmetry operators in Table 1. Upon recentering an atom might not see an identical micro-environment as this particular choice of symmetry operators does not satisfy the first criterion mentioned in the text.

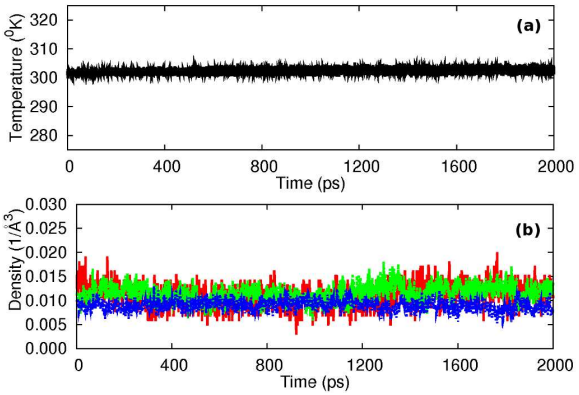

Figure 2: (a) Temprature of solvated viral capsid during 2 ns production period of simulation. (b) Density of heavy atoms of protein within a cylindrical shell of 1 Å width around 3-fold symmetry axis 3f1 with the midpoint of the shell at 5 Å (*red*), 7 Å (*green*) and 9 Å (*blue*).

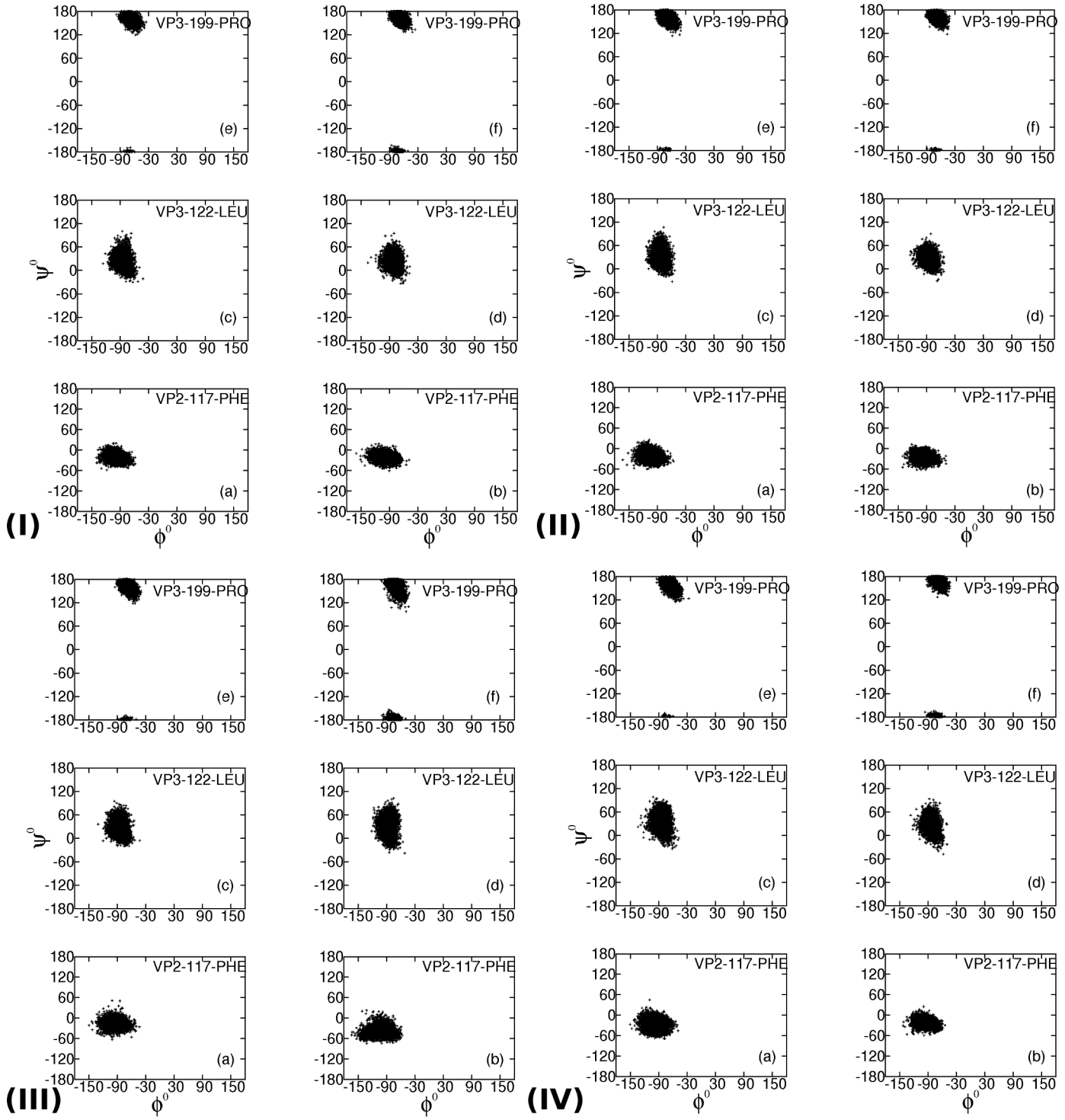

Figure 3: Ramachandran plot of residues closest to 3-fold symmetry axes. The dihedral angles, ϕ and ψ, are plotted for residue 117 of VP2, and residues 122 and 199 of VP3 from protomers located near the 3f1, 3f2 and 3f4 axes (panel *a,c* and *e*), or located near the *3f3* and *3f5* axes (panel *b,d* or *f*). Results are shown for 4 sets of 2 ns production time of simulation - (I), (II), (III) and (IV).